

Liquid Boriding of Cp-Ti and Ti6Al4V Alloy: Characterization of Boride Layers and Tribological Properties

M. Keddam^{a,*}, N. Makuch^b, B. Boumaali^a, A. Piasecki^b, A. Miklaszewski^b, and M. Kulka^b

^aLaboratoire de Technologie des Matériaux, Faculté de Génie Mécanique et Génie des Procédés, Université des Sciences et de la Technologie Houari Boumediene, Bab-Ezzouar, 16111 Algeria

^bInstitute of Materials Science and Engineering, Poznan University of Technology, Poznan, 60-965 Poland

*e-mail: keddam@yahoo.fr

Received May 23, 2019; revised July 12, 2019; accepted July 15, 2019

Abstract—Commercially pure titanium Cp-Ti and Ti6Al4V alloy were liquid borided using a borate bath consisting of 70% borax and 30% SiC at 1000°C for 3, 6, and 12 h. The borided materials were characterized by scanning electron microscopy to reveal the produced microstructures. Two kinds of titanium borides were identified by the X-ray diffraction analysis (TiB₂ on the top of the surface followed by TiB whiskers penetrating into the substrate). The kinetics of formation of titanium borides was also investigated. The hardness of titanium borides was measured by means of the Vickers indenter. The generated Ti borides were characterized by high values of surface hardness. The wear resistance of borided materials (at 1000°C for 12 h) was analyzed by measuring the relative mass loss in comparison with that of the untreated materials. In addition, the wear mechanism was elucidated for both borided and untreated materials. As a result, liquid boriding was found efficient for improving the wear resistance of both materials.

Keywords: liquid boriding, titanium borides, kinetics, wear resistance, tribology

DOI: 10.3103/S1068375520030096

INTRODUCTION

Titanium and its alloys are known for their excellent corrosion resistance. They are widely employed as suitable materials for chemical, marine, and aircraft industry [1] because of their high strength to weight ratio, high stiffness, toughness, and resistance to oxidation. Unfortunately, these materials are characterized by low hardness and poor tribological performance limiting their use if the appreciable resistance to wear is required. To improve the wear resistance of such materials, it is necessary to use the thermochemical treatments such as nitriding [2] or boriding [3–11]. The boriding treatment is an effective thermochemical technique, in which boron atoms diffuse into a workpiece to form hard metal borides.

In practice, various boriding processes were used to harden the surface of titanium and its alloys: laser boriding [3], electrolytic boriding [4–6], boriding in molten salt baths [7], plasma paste boriding [8–11], plasma-assisted boriding [12], and powder-pack boriding [13–19].

In case of titanium and its alloys, two kinds of borides are formed after boriding: TiB₂ and TiB. During the boriding process of such materials, two zones appear: a continuous TiB₂ layer close to the surface and a TiB whiskers layer below the first one.

The aim of this work was to characterize the titanium borides formed on Cp-Ti and Ti6Al4V alloy (coded as TiAl) by the boriding at 1000°C for different times in liquid media, classified as boriding in molten borate baths using reducers without boron [20]. A kinetic study of the liquid boriding of both materials was performed. The wear resistance of the borided materials was evaluated by measuring the relative mass loss. In order to identify the wear mechanisms, the worn surfaces were examined by using an optical microscope.

MATERIALS AND EXPERIMENTAL PROCEDURE

Materials

Two materials were used in the present study as substrates for liquid boriding treatment. Table 1 gives the chemical compositions (in weight percentage) of Cp-Ti and TiAl.

These two specimens were cut from a cylindrical rod and had a diameter of 16 mm and a height of 6 mm.

Liquid Boriding

In recent years, very expensive reducers containing boron (e.g. boron carbide or amorphous boron) were replaced by chemically active metals or their alloys

Table 1. Chemical compositions of Cp-Ti and TiAl (in wt %)

Material	Al	V	Fe	C	Si	O	N	H	Ti
Cp-Ti	—	—	0.05	0.02	—	0.15	0.020	0.001	Balance
TiAl	6.70	4.21	0.10	0.03	0.07	0.14	0.015	0.0003	Balance

with iron (ferroalloys) as well as by silicon carbide (SiC). Therefore, boriding in molten borate baths using reducers without boron became the most popular process in liquid media, excluding the electrochemical boriding [20]. Each specimen was ground up to 1200 grit SiC paper, washed in distilled water, and ultrasonically cleaned in ethyl alcohol before the liquid boriding process. The liquid boriding treatment was carried out in a molten borate bath composed of 70% borax and 30% SiC (as reducing agent without boron) and heated at 1000°C for 3, 6, and 12 h. The salt bath furnace, in which this thermochemical treatment was carried out, possesses an excellent temperature uniformity and ensures a good heat transfer to the treated samples. If SiC was used as reducer [21, 22], the preparation of a bath could be carried out at the ambient temperature without a protective gas. Hence, the boriding process also did not require to use a protective atmosphere (e.g. inert gas) and could be carried out in the unsealed crucible under air atmosphere [20]. After the boriding process, all samples were removed from the furnace, cooled in air, and cleaned from any residues.

X-ray Diffraction Analysis

The titanium borided formed on Cp-Ti and TiAl were identified by the X-ray diffraction (XRD) analysis, using a Philips X-ray diffractometer with a $\text{CuK}\alpha$ radiation ($\lambda_{\text{Cu}} = 0.154 \text{ nm}$) and 2θ angles ranging from 20° to 90° .

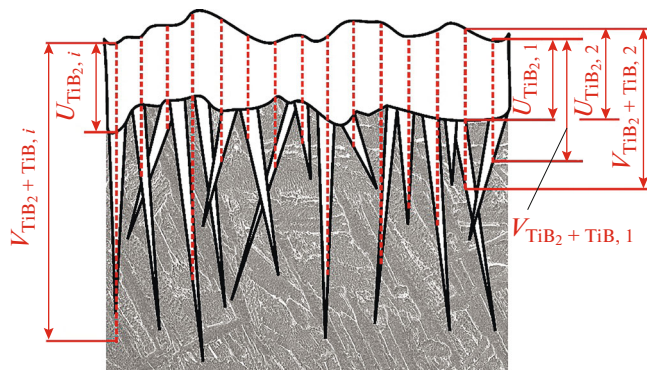


Fig. 1. Principle of measurements of boride layer thickness.

Microstructural Characterization

For the characterization of microstructure, the specimens were prepared using the standard metallographic procedures. First, after the boriding process, the surfaces of borided specimens were cleaned in ethyl alcohol in order to remove the liquid borate solution. After that, the specimens were cut perpendicular to the borided layer with the use of Buehler precision sectioning saw equipped with a borazon cutting disc. Next, the specimens were mounted in a conductive resin KonductoMet. The automatic press Simplimet 1000 Buehler was used for hot mounting. Then, the specimens were ground with SiC abrasive papers of varying granularity (60, 120, 240, 360, 600, 1000, 1500, and 2000). The polishing was carried out using a $0.05 \mu\text{m}$ Al_2O_3 paste and a Phoenix Alpha Grinder/Polisher (Buehler). In order to reveal the microstructure, all of the samples were etched with a mixed acidic solution of HNO_3 , HF, and H_2O , with a volume ratio of 1 : 2 : 47. The cross-sections of borided specimens were observed using a scanning electron microscope (SEM) Tescan Vega 5135 and an optical microscope (OM) Opta Tech LAB 40.

Boride Layer Thickness Measurements

Owing to the special microstructure and morphology of borided layers produced on titanium and its alloy, the method developed and proposed in [23] was applied to measure the thickness of the produced layers. The thickness of a TiB_2 phase U_{TiB_2} and the total thickness of the boride layer $V_{\text{TiB}_2+\text{TiB}}$ were also determined. According to Fig. 1, a hundred measurements ($n = 100$) were taken for each specimen at different equidistant points. The average thickness of a TiB_2 phase U_{TiB_2} was calculated by equation (1):

$$U_{\text{TiB}_2} = \sum_{i=1}^n \frac{U_{\text{TiB}_2,i}}{n} \quad (1)$$

Whereas, the average thickness of the entire layer $\text{TiB}_2 + \text{TiB}$ ($V_{\text{TiB}_2+\text{TiB}}$) was determined as follows:

$$V_{\text{TiB}_2+\text{TiB}} = \sum_{i=1}^n \frac{V_{\text{TiB}_2+\text{TiB},i}}{n} \quad (2)$$

Microhardness Profiles

Microhardness was measured as a function of the distance from the surface. For this study, the etched metallographic specimens were used. The microhard-

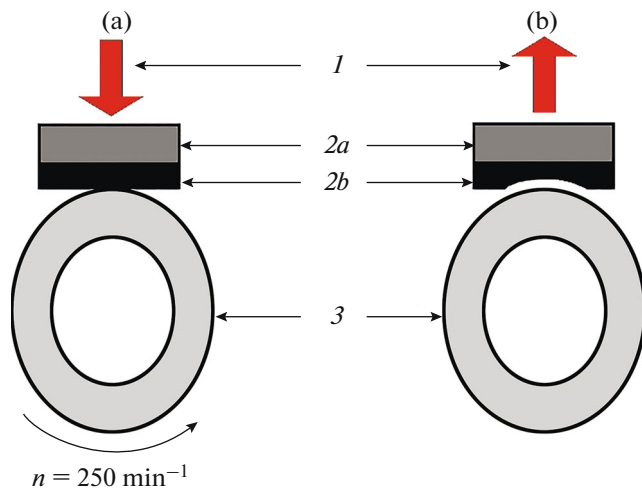


Fig. 2. Scheme of frictional pair: (a) non-conformal contact between specimen and counter-specimen; (b) characteristic deformation of specimen after wear test; (1) test load of 9.81 N; (2a) substrate material; (2b) borided layer; and (3) counter-specimen.

ness tester Micromet II equipped with a Vickers indenter was used. A diamond in the form of a square-based pyramid with an apex angle of 136° was used as indenter. The depth of indentation was about $1/7$ of the diagonal length. The measurements were carried out according to the PN-EN ISO 6507-1 norm. The load of 10 gf (0.0981 N) and a loading time of 15 s were employed during measurements. In order to avoid interaction between the work-hardened regions during measurements, in accordance with the PN-EN ISO 6507-1 norm, the minimum distance between the centers of adjacent indents was $>3d$, where d was the average length of diagonals. For microhardness measurements, the specimens borided at 1000°C (1273 K) for 12 h were used because of the high thickness of the layers produced for these process conditions.

Wear Resistance Tests

The wear resistance tests were performed for the specimens borided at 1000°C (1273 K) for 12 h. The non-borided specimens were also tested for the comparison. The wear resistance tests were arranged as a block-on-ring test using a frictional pair presented in Fig. 2. The specimen in the shape of rectangular prism (2) was stationary during the test and was pressed against the outer surface of a rotating counter-specimen in the shape of ring (3). Obviously, in case of borided specimens, during the wear test, the borided layer (2b) was in the contact with counter-specimens, according to Fig. 2. The investigated samples were in the shape of blocks with dimensions of $12 \times 12 \times 6$ mm. The ring-shaped counter-specimens were made of 100CrMnSi6-4 bearing steel with the following dimensions: the external diameter—20 mm, the internal diameter—12 mm, and the height—12 mm of. As is

shown in Fig. 2a, the specimen and the counter-specimen were in a non-conformal contact. Therefore, if the wear test finished, the characteristic deformation occurred at the surface of specimen, according to Fig. 2b.

The wear resistance tests were performed for 1 h without changes in the counter-specimen under dry sliding conditions at ambient temperature in air using a load of 1 kgf (9.81 N) and a sliding speed of 0.26 m/s corresponding to a sliding distance of 936 m. Before the wear resistance test and after 1 h of test, the specimens were weighed on an analytical balance with an accuracy of ± 0.05 mg.

The wear resistance was evaluated by calculating the relative mass loss $\Delta m/m_i$. The ratio between the mass loss Δm and the initial mass of specimen m_i was determined for the tested specimen according to equation (3):

$$\frac{\Delta m}{m_i} = \frac{m_i - m_f}{m_i}, \quad (3)$$

where Δm is the mass loss (mg); m_i is the initial mass of the specimen (mg); and m_f is the final mass of the specimen (mg).

In order to characterize the wear mechanisms, the worn surfaces were observed using an optical microscope.

RESULTS AND DISCUSSION

Results of X-ray Diffraction Analysis

Figure 3 shows the XRD patterns obtained from the surfaces of the borided materials (Cp-Ti and TiAl) for the boriding parameters as follows: 1000°C and 12 h. Fig. 3 revealed the existence of titanium borides (TiB_2 and TiB) with a change in the values of diffracted intensities. As an obvious fact, there was a detection of peaks of titanium oxide in the XRD patterns of both treated surfaces of Cp-Ti and TiAl. The intensity of these peaks was very low and did not affect the quality of the produced layers. Other researchers reported usage of electrolytic boriding of commercially pure titanium (TA_2) substrate in $\text{Na}_2\text{B}_4\text{O}_7$ –20% K_2CO_3 bath, and they did not detect any peak corresponding to titanium oxide (TiO_2) [4].

Microstructure and Thickness of Layers

For a detailed characterization of the micro-structure of boride layers produced on titanium and TiAl surfaces, SEM imaging of samples borided at 1000°C (1273 K) for 3, 6, and 12 h was carried out, and SEM micrographs are shown in Fig. 4. The produced layers were characterized by the dual-phase microstructure. Near the top-surface, a continuous TiB_2 layer was visible. Below this zone, the TiB whiskers appeared. They penetrated deeper into the base material.

The TiB_2 layers were continuous, dense, and relatively thin in comparison with the range of TiB whiskers, which penetrated deeply into the substrate material. However, it was clearly visible that the TiB whiskers did not grow as a monolithic layer, which results from the presence of a Ti_α phase between the adjacent TiB whiskers. The characteristic directivity of TiB whiskers was explained elsewhere [24]. The growth rate of TiB whiskers along the [010] direction is faster than that perpendicular to the (100), (101), and (001) surfaces. For this reason, a TiB phase is readily to form along the [010] direction to lead to a needle-like morphology, which could tightly combine with the substrate [24]. The average thickness of a TiB_2 layer and the entire layer ($\text{TiB}_2 + \text{TiB}$) calculated for each specimen were compiled in Figs. 5a, 5b, respectively. The kinetics of a TiB_2 layer and of the entire boride layer ($\text{TiB}_2 + \text{TiB}$) obeyed the parabolic growth law. The thickness of the produced layers strongly depended on the duration of the boriding process as well as on the type of the substrate material. Generally, an increase in the duration of liquid boriding resulted in obtaining thicker layers, both in the TiB_2 zone and in the zone with TiB whiskers. Higher layers thicknesses were observed for pure titanium, in comparison to those measured on the borided TiAl. It can be assumed that the presence of alloying elements in TiAl was the reason for more difficult diffusion of boron atoms during boriding. The average depths of penetration of TiB whiskers were calculated based on the method presented in Fig. 1. However, some of them penetrated at a higher depth than the average value. Figures 4a, 4c, 4e, demonstrate that in case of the liquid borided titanium, the obtained maximal depths of TiB whiskers were 30, 55, and 80 μm , respectively. Similarly, for the borided TiAl, the TiB whiskers penetrated at higher depths than the average thickness $V_{\text{TiB}_2+\text{TiB}}$: 25 μm after 3 h of boriding, 55 μm after 6 h, and 80 μm after 12 h. The characteristic morphology and directivity of TiB whiskers could be the reason for a good cohesion of the produced layers with the substrate material.

Other researchers borided the Cp-Ti material between 800 and 1000°C in a salt bath composed of 70% borax and 30% B_4C [7]. The entire boride layer reached a thickness of 30.07 ± 3.1 μm for a treatment time of 12 h. In the present study, the entire boride layer had an average thickness of 42.9 μm at 1000°C for 12 h, by using the mixture of 70% borax and 30% SiC. Hence, the chemical composition of the boride agent for liquid boriding affected the thickness of the entire boride layer.

The entire boride layer formed on TiAl attained an average thickness of 37.9 μm at 1000°C after 24 h of treatment with a TiB_2 layer thickness equal to 5.1 μm . These two layers (TiB_2 and TiB) were produced by pack boriding by using the boriding agent consisting of amorphous boron, anhydrous borax and carbon as filler material [25]. In the present work, the entire boride layer appeared at the surface of TiAl reached an

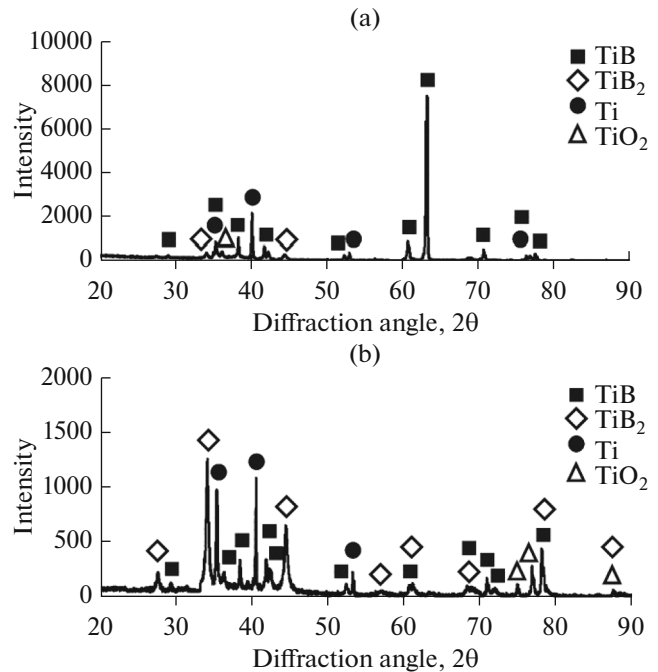


Fig. 3. XRD patterns recorded on the surfaces of liquid borided materials at 1000°C for 12 h: (a) Cp-Ti; (b) TiAl.

average thickness of 26.34 μm for 12 h at the same temperature.

Microhardness Profiles

The OM microstructure and microhardness profile of Cp-Ti borided at 1000°C (1273 K) for 12 h were shown in Fig. 6. The hardness of three zones was analyzed: of a TiB_2 phase, of TiB whiskers region, and of the substrate material. The boundaries between adjacent regions were marked in that figure.

It was clearly visible in Fig. 6 that the total thickness of the boride layer ($\text{TiB}_2 + \text{TiB}$) extends up to 67 μm . This depth was considerably higher than the average thickness of the entire boride layer $V_{\text{TiB}_2+\text{TiB}}$. This situation resulted from the specific method of layer thickness measurements, presented in Fig. 1. The continuous TiB_2 layer was characterized by the highest hardness which ranged from 1790 to 2316 $\text{HV}_{0.01}$. Lower values were obtained near the top-surface, probably due to the rounded edge of the metallographic sample. At the interface between the TiB_2 layer and TiB whiskers, the hardness of about 1500 $\text{HV}_{0.01}$ was measured. In the zone with TiB whiskers, the region with a strong fluctuation in hardness was visible. This situation required an explanation. The characteristic needle-like morphology of TiB whiskers served as the reason that near the TiB_2 zone, the TiB whiskers were characterized by a larger width. In some areas, up to a depth of 20 μm from the surface, the width of a single TiB whisker reached even 5 μm . For this reason, it was

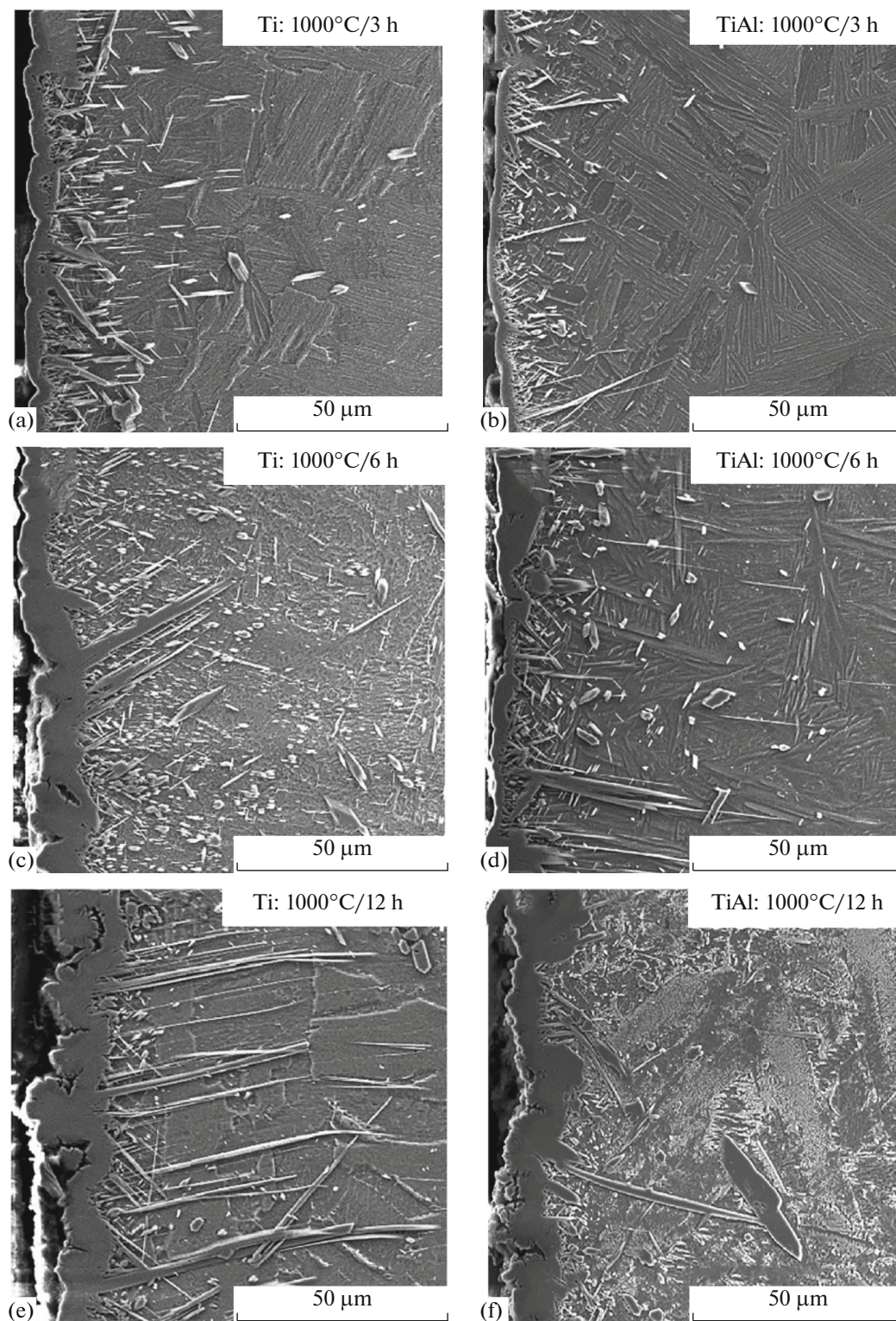


Fig. 4. SEM images of microstructures of liquid borided layers produced on: (a, c, and e) titanium; and (b, d, and f) on TiAl: using various process parameters.

possible to measure the hardness only in the TiB needle, because the produced indentation mark was smaller than the width of the tested needle. In these

areas, in which indentation was performed in a TiB whisker, a higher hardness of 1500 HV_{0.01} was obtained. Simultaneously, a lower hardness corre-

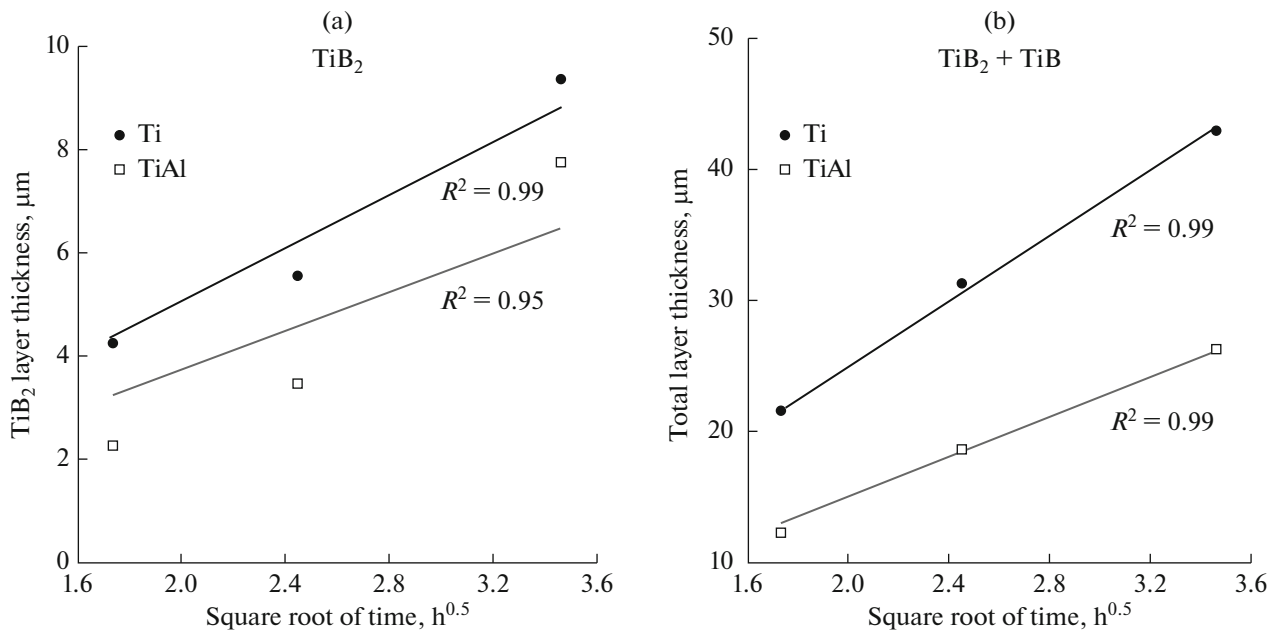


Fig. 5. Time dependence of average thicknesses of TiB₂ layer and entire boride layer: (a) TiB₂, and (b): (TiB₂+TiB).

sponded to the areas in which the hardness was measured in both TiB whisker and the adjacent Ti_α substrate material. Obviously, the presence of the substrate material resulted in diminished hardness (1486–1074 HV_{0.01}). In the substrate material, the lowest hardness was measured to be about 290 HV_{0.01}.

The OM microstructure and microhardness profile of the borided TiAl at 1000°C (1273 K) for 12 h were shown in Fig. 7. Likewise to the results obtained for the borided titanium, three regions could be observed: the continuous TiB₂ phase near the top-surface, below it—a TiB whiskers region, and that of the substrate material.

A high hardness ranged from 1652 to 2211 HV_{0.01}, which corresponded to that of the continuous TiB₂ layer. In the second tested region, the mixture of TiB whiskers and the titanium matrix occurred. For this reason, near the TiB₂ region, at the distance of 18 μm from the surface, a higher hardness of 1547 HV_{0.01} was obtained. This measurement was performed in a single TiB whisker. Obviously, an increase in the distance from the surface caused a decrease in width of TiB whiskers due to its specific needle-like morphology. As a result, the tested areas contained higher amounts of the substrate material, which caused a diminished hardness ranged from 467 to 1235 HV_{0.01}. At the end of the TiB whiskers region, the percentage of the substrate material between the adjacent whiskers was high, whereas the width of whiskers was low. Therefore, the hardness obtained at a depth of 38 μm from the surface was only slightly higher than that of the base material (average value of 270 HV_{0.01}).

The microhardness of TiB₂ and TiB phases obtained for boride layers produced by the use of different boriding techniques is presented in Table 2. The results obtained in the present study were comparable to those described elsewhere [5, 9, 12, 15, 16, 24, 29]. In the borided layers produced on titanium and its alloys, the zones were visible as follows: a compact TiB₂ layer, a TiB₂ + TiB subsurface layer, and TiB whiskers together with the substrate material. Obviously, each phase had different hardness. In all cases, a higher hardness was measured for a compact and homogenous TiB₂ layer. Whereas, a lower hardness was characteristic of TiB whiskers, especially if the percentage of the substrate material in the tested area was relatively high. An extremely high hardness of the TiB₂ region was measured and reported in [24, 26]. The authors in [24] have produced the dual-phase layer on the pure titanium as a result of liquid boriding. The molten salt bath was composed of: an amorphous boron in 10%, borax in 70%, pure Al in 10% as a reducing agent and KCl in 10% as an activator. The microhardness profile indicated an increase in hardness up to 3000–3500 HV in a TiB₂ phase. Below, a subsurface layer with a TiB₂ phase and TiB whiskers was detected. This zone was characterized by the diminished hardness in a range of 1800–3000 HV. The lowest hardness was measured in the TiB-Ti region (400–1800 HV). The authors in [26] have pack-borided the commercially pure titanium (grade-2) and measured the microhardness profile through the boride layer obtained at 950°C for 24 h. A maximal value of the surface hardness by Vickers indentation was about 4100 ± 300 HV_{0.01} under a load of 10 gf and corresponding to that of the the TiB₂ layer. So, the

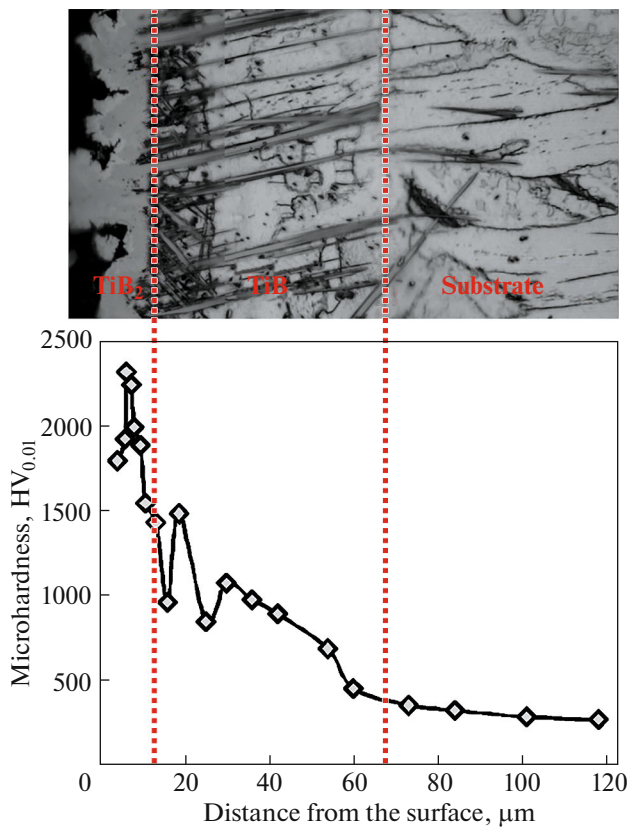


Fig. 6. OM microstructure and microhardness profile of borided Cp-Ti at 1000°C (1273 K) for 12 h.

hardness values obtained in [24, 26] were higher than those measured in the present study. The differences could result from the specific surface topography. As is vivid in Fig. 6, the top surface of the borided Cp-Ti at 1000°C (1273 K) for 12 h was characterized by a relatively high inhomogeneity. The edge of the specimen was not smooth. These factors strongly influenced the results of the hardness test because it was difficult to generate a high-quality indentation mark near the top surface.

Wear Resistance Results

The wear resistance of both borided and untreated specimens was determined based on the calculation of the relative mass loss $\Delta m/m_i$. The results are depicted in Fig. 8. Due to the presence of hard titanium borides, the borided specimens were characterized by about five-time lower $\Delta m/m_i$ ratio in comparison with that of non-borided specimens. Both the borided titanium and the borided TiAl consisted of a dual-phase layer ($\text{TiB}_2 + \text{TiB}$ whiskers). To sum up here, similar results were obtained for these specimens. The untreated TiAl was characterized by a slightly lower wear resistance in comparison with that of the untreated pure titanium.

Figure 9 shows OM micrographs of worn surfaces of non-borided specimens of pure titanium and of

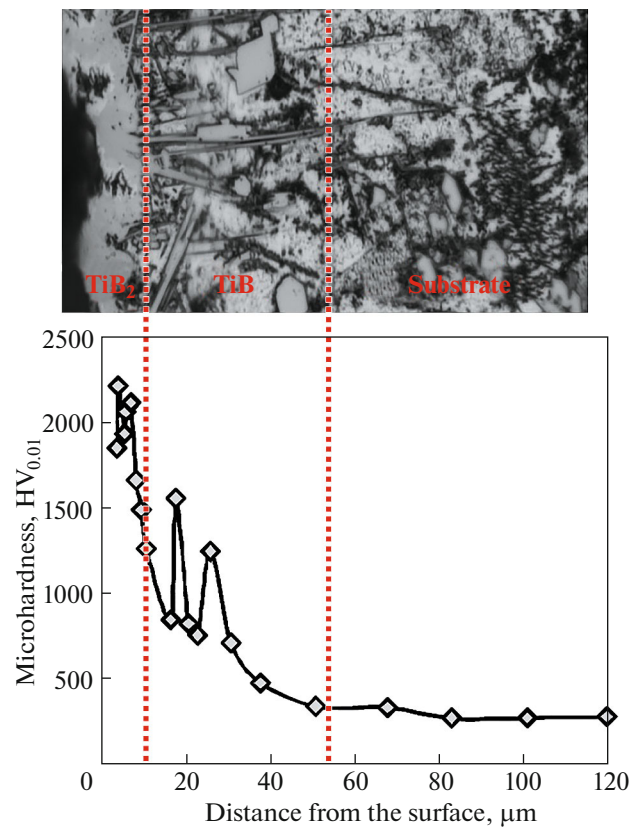


Fig. 7. OM microstructure and microhardness profile of TiAl borided at 1000°C (1273 K) for 12 h.

TiAl. In Figs. 9a, 9d, the presence of severe plastic deformation could be observed for both untreated materials. The plastic deformation occurred along the sliding direction. Simultaneously, the worn surfaces of both titanium and TiAl were characterized by the presence of grooves parallel to the sliding direction, formed during the test (Figs. 9b, 9e). Some visible effects of spalling were also detected in Figs. 9c, 9f. This spalling could be caused by the wear particles removed from the contact surface. It could be concluded that the wear mechanism for non-borided pure titanium and for TiAl was a mixing one of the primary plastic deformation and the secondary abrasive wear.

The OM micrographs of worn surfaces of borided pure titanium and TiAl alloy after 1 h of wear resistance test are presented in Fig. 10. Due to high hardness of titanium boride layers and to a low test load of 9.81 N, the plastic deformation of these specimens was limited (Figs. 10a, 10c). Unfortunately, continuous TiB_2 layers produced on the surface of both titanium and TiAl were relatively thin. Simultaneously, the surface after boriding was characterized by some irregularity. These two factors served the reason why in the end of tribological tests, in some areas, the titanium boride layer began to be damaged. After that, the wear fragments of the boride layer peel off from the contact surface, and the titanium substrate was exposed. How-

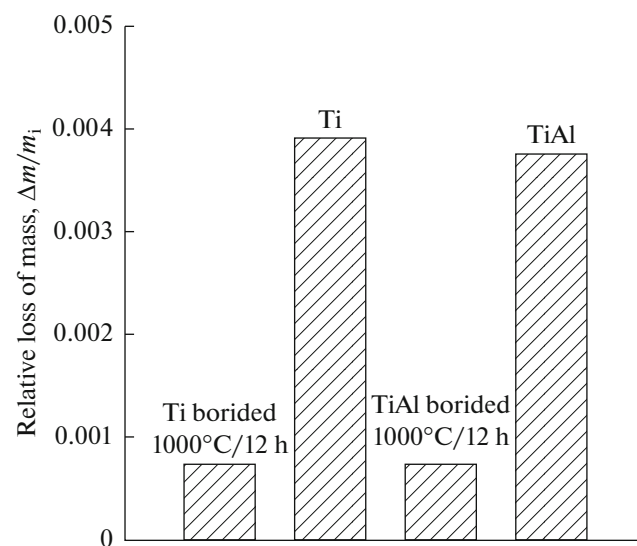
Table 2. Microhardness of borided layers produced on titanium and its alloys via different boriding techniques

Ref.	Material	Boriding technique	Microhardness
[5]	Pure Ti	Electrochemical	TiB ₂ : 32 ± 1.5 GPa TiB whiskers: 15 ± 5 GPa
[9]	Pure Ti	Plasma-paste	TiB ₂ : 1811–2452 HV TiB + Ti: 467–1703 HV
[12]	TiAl	Plasma-assisted	TiB ₂ + TiB: 2500–2800 HK
[15]	TiAl	Powder-pack	TiB ₂ + TiB: 1500–2700 HV TiB + Ti: 400–1500 HV
[16]	TB2 alloy	Powder-pack	TiB ₂ : 23–27.50 GPa TiB whiskers: 13–23 GPa
[24]	Pure Ti	Liquid	TiB ₂ : 3000–3500 HV TiB ₂ + TiB: 1800–3000 HV TiB + Ti: 400–1800 HV
[26]	Pure Ti	Powder-pack	TiB ₂ : 4100 ± 300 HV TiB ₂ + TiB: 2000 ± 500 HV TiB + Ti: 1500 HV
[29]	TiAl	Powder-pack	TiB ₂ : 25–28.40 GPa TiB + Ti: 3.42–14.89 GPa
This work	Pure Ti	Liquid	TiB ₂ : 1790–2316 HV TiB ₂ + TiB interface: 1500 HV TiB + Ti: 1074–1486 HV
	TiAl	Liquid	TiB ₂ : 1652–2211 HV TiB interface: 1547 HV TiB + Ti: 467–1235 HV

ever, the visible effects of intensive abrasive wear were also detected in the borided titanium (Fig. 10b) and the borided TiAl (Fig. 10d). The wear mechanism of the borided specimens changed from an abrasive wear with visible grooves to an adhesive wear with visible effects of spalling. Obviously, in the areas in which the substrate material was not exposed, the predominant wear mechanism was abrasive wear. The spalling of titanium boride layer occurred only in areas in which its continuity was interrupted, and the substrate material was exposed. It could be concluded that liquid boriding provided a suitable protection against wear for both titanium and TiAl. The presence of the titanium borides layer on the top surface caused also limited plastic deformation of the base material.

The obtained results of wear tests proved an increased wear resistance of both borided Cp-Ti, and TiAl. The calculated relative mass loss was about five-time lower in comparison with that of the unborided specimen. However, it was difficult to compare the obtained results to the literature data because of differences in the methodology of the wear resistance tests (load, time duration, type of counter-specimen, type of test, and friction pair shape). Excellent tribological properties of titanium borides were described by many authors [9, 15, 24, 26]. An increase in wear resistance was a result of producing hard boride layers with the

use of different boriding techniques. In the case of the powder-pack borided TiAl under both dry and smear lubrication sliding conditions, the superior tribologi-

**Fig. 8.** Relative mass loss of specimens $\Delta m/m_i$ after wear resistance test.

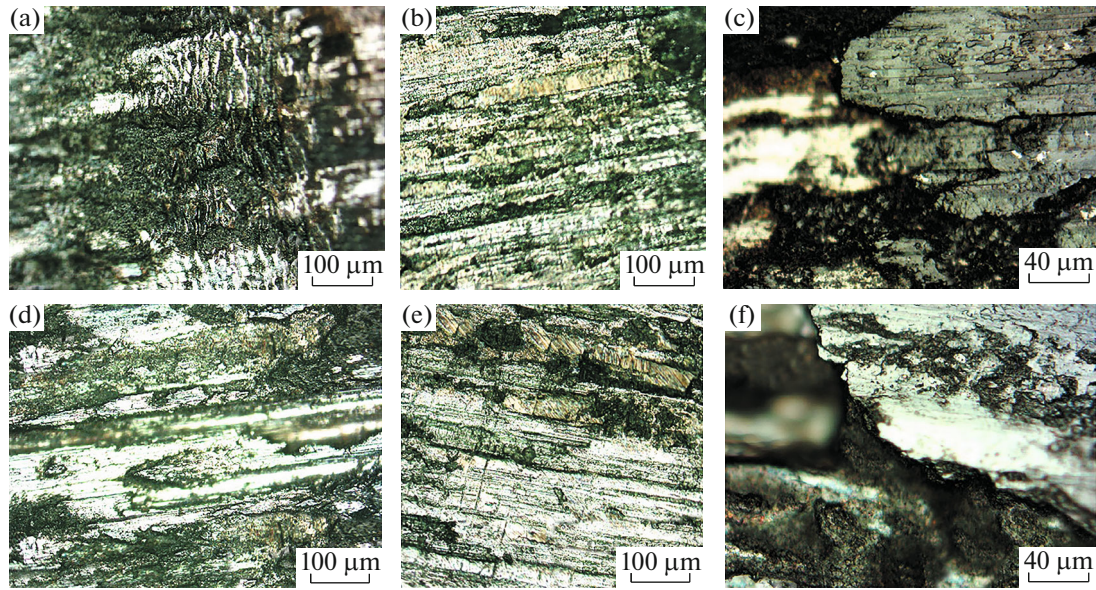


Fig. 9. Worn surfaces of non-borided specimens after wear resistance test: (a, b, and c) non-borided titanium; (d, e, and f) non-borided TiAl.

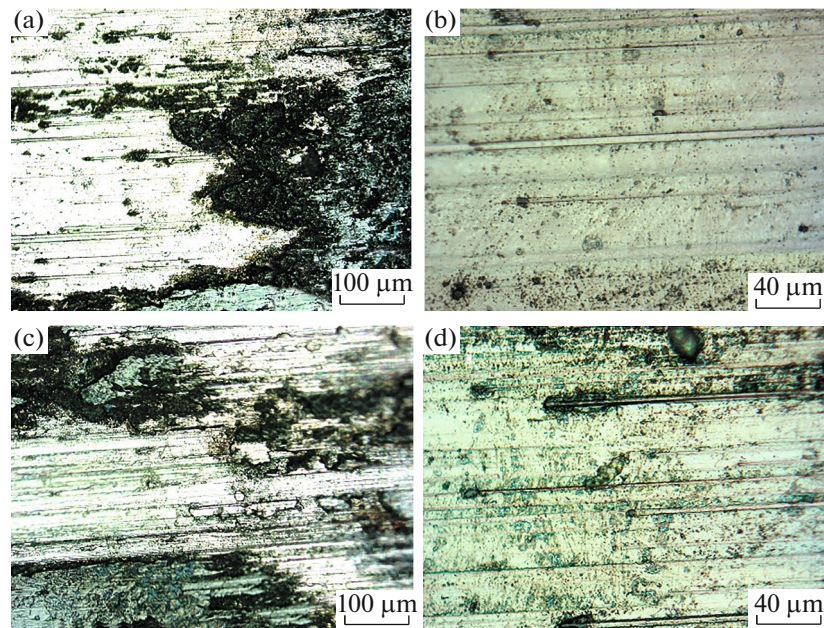


Fig. 10. Worn surfaces of liquid borided specimens after wear resistance test: (a, b) borided titanium; and (c, d) borided TiAl tribological performance of the liquid borided titanium and TiAl.

cal performance against a sapphire ball was obtained. Both a relative wear rate and a friction coefficient were significantly lower in comparison with those of the untreated alloy [15]. Promising tribological properties were also obtained after molten salt boriding of Cp-Ti described in [24]. The borided specimens showed an improved wear resistance compared to that of the untreated Cp-Ti under dry sliding conditions with

10 N normal load. The differences in the wear mechanisms for both specimens were also found. The wear mechanism of Cp-Ti was revealed as the adhesive wear and the abrasive wear. Whereas for the borided sample, the wear mechanism was identified as the micro-cuts wear [24]. Wear resistance of the plasma-paste borided layers produced on pure Ti was even 9 times higher compared to that of the untreated Cp-Ti [9].

The value of the relative mass loss of the borided specimens strongly depended on the parameters of the plasma paste boriding. An increased temperature and duration of the process resulted in an increase in wear resistance [9]. The researchers in [26] carried out wear tests under non lubricating conditions by using a pin-on-disk tribometer on both untreated and borided Cp-Ti materials. Severe plastic deformation characterized by scratches and grooves was observed on the untreated Cp-Ti material while the worn surfaces of borided samples exhibited a very limited plastic deformation with smearing effects. The wear resistance tests results obtained in the present study confirmed the good tribological performance of the liquid borided titanium and TiAl.

CONCLUSIONS

In this work, the liquid boriding in the molten borate bath consisting of 70% borax and 30% SiC was carried out on Cp-Ti and TiAl at a temperature of 1000°C for 3, 6 and 12 h.

The following concluding points were drawn:

—For all of the boriding conditions and for both treated materials, a continuous and dense TiB₂ layer was formed, and, underneath it, a TiB whiskers layer occurred exhibiting a difference in thickening and length.

—The XRD analysis confirmed the presence of two types of titanium borides: TiB₂ and TiB.

—The Vickers indentation measurements showed for the TiB₂ layer the highest hardness ranging from 1790 to 2316 HV_{0.01}.

—The thicknesses of the entire boride layers varied with the treatment time in a range of 21.56–42–91 μm for the borided Cp-Ti and between 12.28 and 26.34 μm for the borided TiAl at 1000°C. The kinetics of the TiB₂ layer and of the entire boride layer obeyed the parabolic growth law.

—Both borided Cp-Ti and TiAl exhibited a lower, about five-fold, relative mass loss compared to that of the untreated samples.

—The untreated TiAl showed a slightly lower wear resistance in comparison with that of the untreated Cp-Ti.

—The wear mechanism of the borided Cp-Ti and TiAl was of a mixed nature. It changed from abrasive wear with visible grooves to adhesive wear with an evident effect of spalling.

—The liquid boriding treatment improved the wear resistance of both materials: Cp-Ti and TiAl.

CONFLICT OF INTEREST

The authors declare to have no conflict of interest.

REFERENCES

- Lutjering, G. and Williams, J.C., *Titanium*, Berlin: Springer-Verlag, 2007.
- Zhecheva, A., Malinov, S., and Sha, W., *JOM*, 2007, vol. 59, pp. 38–40.
- Badini, C., Bianco, M., Talentino, S., Guo, X.B., et al., *Appl. Surf. Sci.*, 1992, vol. 54, pp. 374–380.
- Huang, Y.G., Chen, J.R., Zhang, M.I., Zhong, et al., *Mater. Manuf. Processes*, 2013, vol. 28, pp. 1310–1313.
- Kartal, G., Timur, S., Urgen, M., and Erdemir, A., *Surf. Coat. Technol.*, 2010, vol. 204, pp. 3935–3939.
- Çelikkan, H., Öztürk, M.K., Aydin, H., and Aksu, M.I., *Thin Solid Films*, 2007, vol. 515, pp. 5348–5352.
- Boumaali, B., Keddad, M., and Taktak, S., *Int. J. Mater. Eng. Innovation*, 2018, vol. 9, pp. 240–255.
- Ataibis, V. and Taktak, S., *Surf. Coat. Technol.*, 2015, vol. 279, pp. 65–71.
- Makuch, N., Kulka, M., Keddad, M., Taktak, S., et al., *Thin Solid Films*, 2017, vol. 626, pp. 25–37.
- Keddad, M. and Taktak, S., *Appl. Surf. Sci.*, 2017, vol. 399, pp. 229–236.
- Keddad, M., Taktak, S., and Tasgetiren, S., *Surf. Eng.*, 2016, vol. 32, pp. 802–808.
- Kaestner, P., Olfe, J., and Rie, K.T., *Surf. Coat. Technol.*, 2001, vols. 142–144, pp. 248–252.
- Tikekar, N.M., Ravi Chandran, K.S., Sanders, A., *Scr. Mater.*, 2007, vol. 57, pp. 273–276.
- Lee, C., Sanders, A., and Tikekar, N., Ravi, et al., *Wear*, 2008, vol. 265, pp. 375–386.
- Atar, E., Kayali, E.S., and Cimenoglu, H., *Surf. Coat. Technol.*, 2008, vol. 202, pp. 4583–4590.
- Li, P., Liu, D., Bao, W., Ma, M., et al., *Ceram. Int.*, 2018, vol. 44, pp. 18429–18437.
- Peng, M.J., Duan, Y.H., Ma, L.S., and Shu, B.P., *J. Alloys Compd.*, 2018, vol. 769, pp. 1–9.
- Kaplan, Y., Cetin Can, A., and Ulukoy, A. *Proc. Inst. Mech. Eng., Part L*, 2016, vol. 0, pp. 1–11.
- Ivanov, S.G., Guriev, M.A., Loginova, M.V., Deev, V.B., et al., *Russ. J. Non-Ferrous Met.*, 2017, vol. 58, pp. 244–249.
- Kulka, M., *Current Trends in Boriding*, New York: Springer-Verlag, 2019.
- Allaoui, O., Bouaouadja, N., and Saindeman, G., *Surf. Coat. Technol.*, 2006, vol. 201, pp. 3475–3482.
- Bouaziz, S.A., Boudaoud, N., and Zanoun, A., *Mater. Tech.*, 2009, vol. 97, pp. 253–259.
- Kunst, H. and Schaaber, O., *Haertere-Tech. Mitt.*, 1967, vol. 22, pp. 1–25.
- Ma, L.S., Duan, Y.H., and Li, P., *J. Mater. Eng. Perform.*, 2017, vol. 26, pp. 4544–4555.
- Kara, G. and Purcek, G., *Surf. Eng.*, 2019, vol. 35, pp. 611–617.
- Kara, G., Purcek, G., and Yanar, H., *Ind. Lubr. Tribol.*, 2017, vol. 69, pp. 65–70.
- Munro, R.G., *J. Res. Natl. Inst. Stand. Technol.*, 2000, vol. 105, pp. 709–720.
- Zhu, Y.S., Lu, W.Z., Zuo, D.W., Feng, W., et al., *Surf. Eng.*, 2014, vol. 30, pp. 612–618.
- Duan, Y., Li, P., Chen, Z., Shi, J., et al., *J. Alloys Compd.*, 2018, vol. 742, pp. 690–701.